International Journal of
MATERIALS RESEARCH

Zeitschrift für METALLKUNDE

Original Contributions

Boris B. Straumal[a,b,c], Askar R. Kilmametov[b], Yulia Ivanisenko[b], Andrei A. Mazilkin[a,b], Olga A. Kogtenkova[a], Lilia Kurmanaeva[d], Anna Korneva[e], Pawel Zięba[e], Brigitte Baretzky[b]

[a] Institute of Solid State Physics, Russian Academy of Sciences, Chernogolovka, Russia
[b] Karlsruher Institut für Technologie, Institut für Nanotechnologie, Eggenstein-Leopoldshafen, Germany
[c] Laboratory of Hybrid Nanomaterials, National University of Science and Technology "MISIS", Moscow, Russia
[d] Institute of Metallurgy Department of Chemical Engineering & Materials Science, University of California, Davis, USA
[e] Institute of Metallurgy and Materials Science, Polish Academy of Sciences, Cracow, Poland

Phase transitions induced by severe plastic deformation: steady-state and equifinality

Paper presented at "XV International Conference on Electron Microscopy", 15–18 September 2014, Cracow, Poland

International Journal of Materials Research downloaded from www.hanser-elibrary.com by KIT - Karlsruher Institut für Technologie on July 11, 2015
For personal use only.

During severe plastic deformation (SPD), a steady-state is usually reached after a certain value of strain (i.e. number of passes during equal-channel pressing or number of rotations during high pressure torsion). The structure and properties of a material in a steady state (including composition of phases) do not depend on those in the starting state before SPD. In other words they are equifinal, and the production of lattice defects is in dynamic equilibrium with defect elimination. Moreover, the SPD-treatment at ambient temperature $T_{SPD} = 300$ K is frequently equivalent to the heat treatment at a certain elevated temperature $T_{eff} > 300$ K. For example, the composition of phases in Cu–Ni, Co–Cu and Nd–Fe–B-based alloys after high pressure torsion corresponds to the states at 200, 890 and 1 170 °C, respectively, and is rather insensitive to the high pressure torsion rate (between 0.2 and 2 rpm) and pressure (between 3 and 8 GPa).

Keywords: Phase transitions; Severe plastic deformation; Steady-state; Equifinality

1. Introduction

Severe plastic deformation (SPD) frequently leads to phase transformations in materials [1–4]. In other words, the phases before SPD and after this treatment are different. SPD can drive the formation [5–12] or decomposition [13–15] of a supersaturated solid solution, the dissolution of phases [16–28], disordering of ordered phases [19–31], amorphization of crystalline phases [32–40], synthesis of the low-temperature [21, 28], high-temperature [41–43] or high-pressure [44–52] allotropic modifications, and nanocrystallization in the amorphous matrix [53–61]. Quite frequently, the phases after SPD are the same as phases which would appear in a material after long annealing at a certain (elevated) temperature. This temperature is called the effective temperature T_{eff}. According to the idea of Martin, in the case of amorphization or a mixture of amorphous and crystalline phases, the effective temperature T_{eff} can be found in the equilibrium phase diagrams in the areas where the liquid phase exists or co-exists with crystalline phase(s) [62, 63].

The important feature of SPD is that a material is deformed under high hydrostatic pressure and fracture cannot take place even after the introduction of a high density

International Journal of Materials Research downloaded from www.hanser-elibrary.com by KIT - Karlsruher Institut für Technologie on July 11, 2015
For personal use only.

of lattice defects. As a result, after a certain strain the steady state is reached during SPD when structure and properties of a material do not change any more with increasing strain, such as the number of passes during equal-channel pressing or number of anvil rotations during high pressure torsion (HPT). The steady state during SPD means that the rate of production of lattice defects by an external mechanical force becomes equal to the rate of elimination of these defects. For the conventional thermomechanical treatments (when fracture is geometrically possible) such dynamic equilibrium can appear only at elevated temperatures.

It is important that the dynamic equilibrium during SPD takes place at temperature T_{SPD} (which usually remains slightly above the ambient one) when lattice diffusion is frozen and conventional diffusion relaxation is impossible. Nevertheless, the SPD-treatment at T_{SPD} usually leads to very quick phase transformations, which is easy to understand if one considers the high density of defects, similar to an increased temperature. The increased pressure, oppositely, leads to the decrease of diffusivity and/or grain boundary mobility [64, 65]. For a pressure of 5 GPa the bulk diffusion coefficient drops by about 2–3 orders of magnitude, the grain boundary (GB) diffusivity decreases by 8–15 orders of magnitude (dependent on the GB misorientation and inclination) [64], the GB mobility becomes 2–8 orders of magnitude lower [65]. Some SPD-driven phase transformations need only a small shift of atoms, for other ones long-range mass transfer is needed. The results of such SPD-driven transitions cannot be explained by the bulk or even grain boundary diffusion at the SPD temperature. For several systems it has been shown that the structure and properties of a material in a steady state do not depend on those in the starting state before SPD [66]. In other words they are equifinal [67]. In this paper we discuss certain important features of steady state during HPT with and without amorphization of a starting material.

2. Experimental procedure

Cu–Ni, Cu–Co and Nd–Fe–B-based alloys of various compositions were investigated. The Cu–Ni and Cu–Co alloys were prepared from high purity components by means of vacuum induction melting. The melts were poured under vacuum into a water-cooled cylindrical copper crucible of 10 mm diameter. Nd–Fe–B-based liquid-phase sintered alloy was purchased from the company Vacuumschmelze GmbH (Germany): it contained 66.5 wt.% Fe, 22.1 wt.% Nd, 9.4 wt.% Dy, 1.0 wt.% Co, 0.8 wt.% B, 0.2 wt.% Cu. For HPT processing, 0.6 mm thick discs were cut from the as-cast ingots, then ground and chemically etched. The discs of Cu-4.9 wt.% Co and Cu-77 wt.% Ni alloys were sealed into evacuated silica ampoules with a residual pressure of approximately 4×10^{-4} Pa at room temperature. The sealed ampoules with Cu-4.9 wt.% Co discs were solution treated at 1060 °C for 10 h and precipitation treated at 570 °C for 840 h. The ampoules with Cu-77 wt.% Ni discs were homogenized at 850 °C for 500 h. After annealing they were quenched in water. The accuracy of the annealing temperature was ±1 °C. After sawing, grinding, and chemical etching, the 0.7 mm thick discs cut from the as cast Nd–Fe–B-based alloys cylinders and annealed Cu–Ni and Cu–Co discs were subjected to HPT in a Bridgman anvil type unit (room temperature, pressure 5 GPa, 5 torsions, 1 rotation-per-minute) using a custom-built computer controlled HPT device (W. Klement GmbH, Lang, Austria). After HPT, the central (low-deformed) part of each disc (about 3 mm in diameter) was excluded from further investigations. The samples for structural investigations were cut from the deformed discs at a distance of 4–5 mm from the sample centre. Scanning electron microscopy (SEM) investigations were carried out in a Tescan Vega TS5130 MM microscope equipped with a LINK energy-dispersive spectrometer and on a Philips XL30 scanning electron microscope equipped with a LINK ISIS energy-dispersive spectrometer produced by Oxford Instruments. Transmission electron microscopy (TEM, HRTEM, STEM, EDXS) studies were carried out on TITAN 60-300 instrument, TECNAI F2 electron microscope with acceleration voltage of 200 kV and on a PHILIPS CM20 microscope at an accelerating voltage of 200 kV. X-ray diffraction (XRD) data were obtained on a Siemens diffractometer (Co-K_α radiation). Grain (crystallite) size was estimated by the XRD line broadening and using the Scherer formula.

3. Results and discussion

Figure 1 shows the dependence of torsion torque on the rotation angle (strain) for the Cu-4.9 wt.% Co alloy in two states (Fig. 1a) and for the as-delivered Nd–Fe–B-based alloys (Fig. 1b). The Cu-4.9 wt.% Co alloy was in two states, namely after annealing at 1060 °C for 10 h and after annealing at 570 °C for 840 h. In the first case Co was fully dissolved in Cu because the solubility of Co in Cu at 1060 °C is about 8 wt.% Co [68]. In the second case the Cu-based solid solution almost fully decomposed: less than 0.5 wt.% Co remained dissolved in Cu (based on XRD measurements and the phase diagram [68]). It can be clearly seen that the torsion torque in the Cu-4.9 wt.% Co alloy in both states becomes almost constant after about 0.5 anvil rotations (Fig. 1a). The torsion torque in Al alloys also becomes stationary after about 0.5–1 rotation [69]. The Nd–Fe–B-based alloy behaves slightly differently (Fig. 1b). After a quick starting increase of torsion torque from zero to ~250 N·m, a slow work hardening takes place. The torsion torque linearly increases until ~2.5 anvil rotations. After this point the torsion torque stabilizes between 370 and 390 N·m. The Nd–Fe–B-based alloy is much harder than the studied Cu–Co alloy; therefore, the steady state value of torsion torque for the Nd–Fe–B-based alloy (Fig. 1b) is about four times higher than that of Cu-4.9 wt.% Co alloy (Fig. 1a). Moreover, the slow hardening stage is absent in the curve for fully crystalline Cu-4.9 wt.% Co alloy (Fig. 1a). In our opinion, the slow hardening appears during amorphization of the Nd–Fe–B-based alloy.

As usual [70, 71], HPT of both Cu-4.9 wt.% Co alloys and of homogenized Cu-77 wt.% Ni alloy leads to strong grain refinement (Figs. 2 and 3). The grain size d before HPT was between 50 and 500 μm [66, 72]. After HPT the grain size d measured by TEM was about 200 nm in both Cu-4.9 wt.% Co alloys (Fig. 2) and about 150 nm in the Cu-77 wt.% Ni alloy (Fig. 3). The grain size in pure copper after HPT (5 rotations after 6 GPa) measured by TEM was between 100 and 300 nm [73]. A similar grain size in pure copper after HPT (200–300 nm) was observed by TEM

International Journal of Materials Research downloaded from www.hanser-elibrary.com by KIT - Karlsruher Institut für Technologie on July 11, 2015
For personal use only.

also in Ref. [74]. XRD of the same samples gave the crystallite size (or the size of coherently scattered domains) of 50 nm after HPT at 4 GPa and 70 nm after 2 GPa [74]. Careful TEM investigation of pure Cu (HPT, 5 rot, 7 GPa) permitted observation of rather large grains with size of 100–200 nm containing elongated 10–20 nm small subgrains as well as a certain amount of very fine equiaxed grains with a size of 10–20 nm [75]. The addition of a second component to pure copper usually leads to smaller grain size after SPD, as in Cu–In alloys [76]. The smaller grain size in Cu-77 wt.% Ni alloy in comparison with Cu-4.9 wt.% Co alloy correlates with this tendency. Such a decrease in grain size has also been observed in alloys exhibiting solution hardening after ball milling [3]. In this work the GBs in Cu–Co and Cu–Ni alloys after HPT are thin and well-defined (with thickness about 2–3 nm and abrupt orientation contrast in dark field TEM images between neighbouring grains) as they always are in HPT-treated Cu-alloys with positive mixing enthalpy [2, 15, 66, 77]. In contrast, in the Cu–In alloys with negative mixing enthalpy the grain boundaries are broad and less-defined (their thickness reaches 10–15 nm where one grain continuously

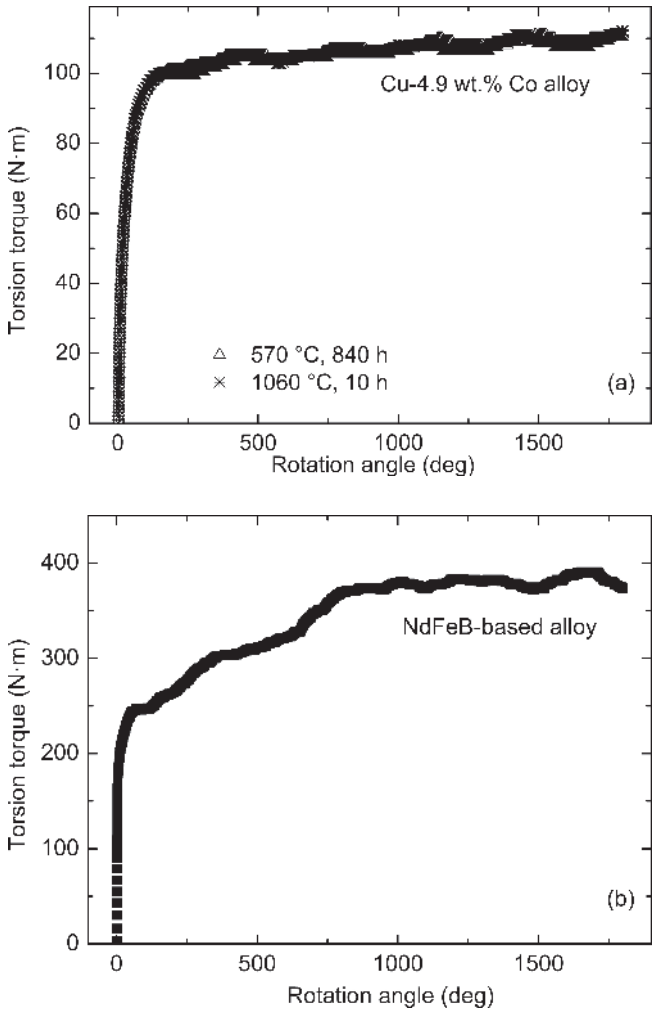

Fig. 1. Dependence of HPT torsion torque on the rotation angle. (a) For the Cu-4.9 wt.% Co alloy after annealing at 570 °C for 840 h (open triangles) and at 1060 °C for 10 h (stars). (b) For the as-delivered commercial Nd–Fe–B-based alloy.

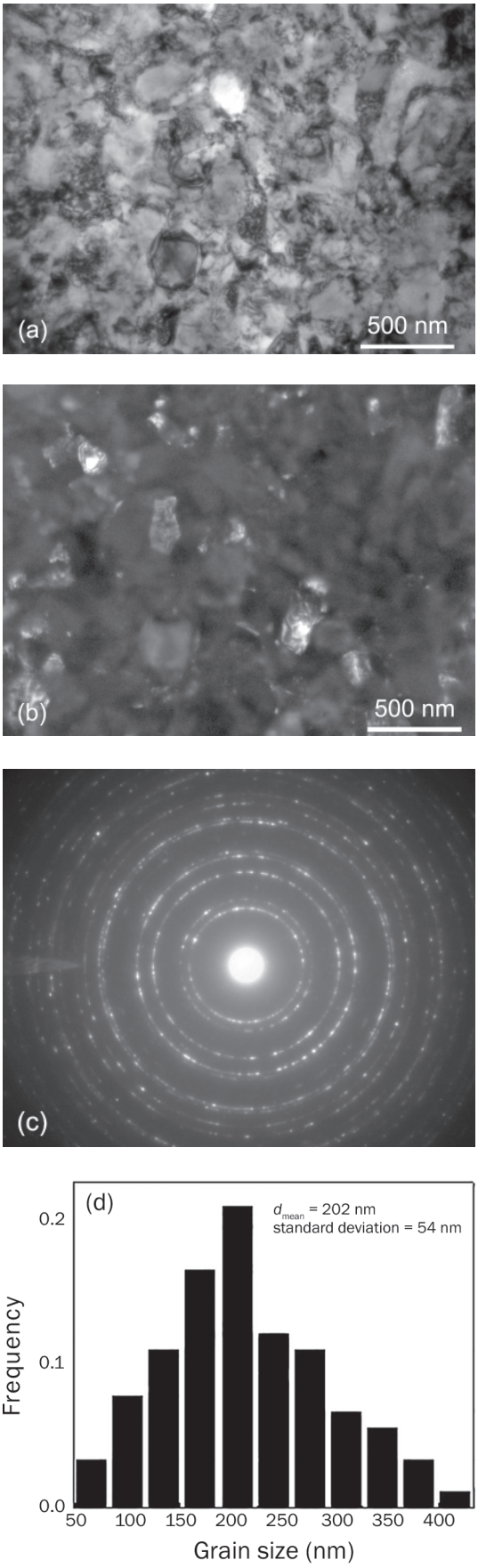

Fig. 2. TEM micrographs of Cu-4.9 wt.% Co alloy annealed at 1060 °C for 10 h after HPT (5 GPa, 5 rot, 1 rpm): (a) Bright field; (b) Dark field; (c) Diffraction pattern. (d) Histogram for the distribution of grain size *d*.

International Journal of Materials Research downloaded from www.hanser-elibrary.com by KIT - Karlsruher Institut für Technologie on July 11, 2015
For personal use only.

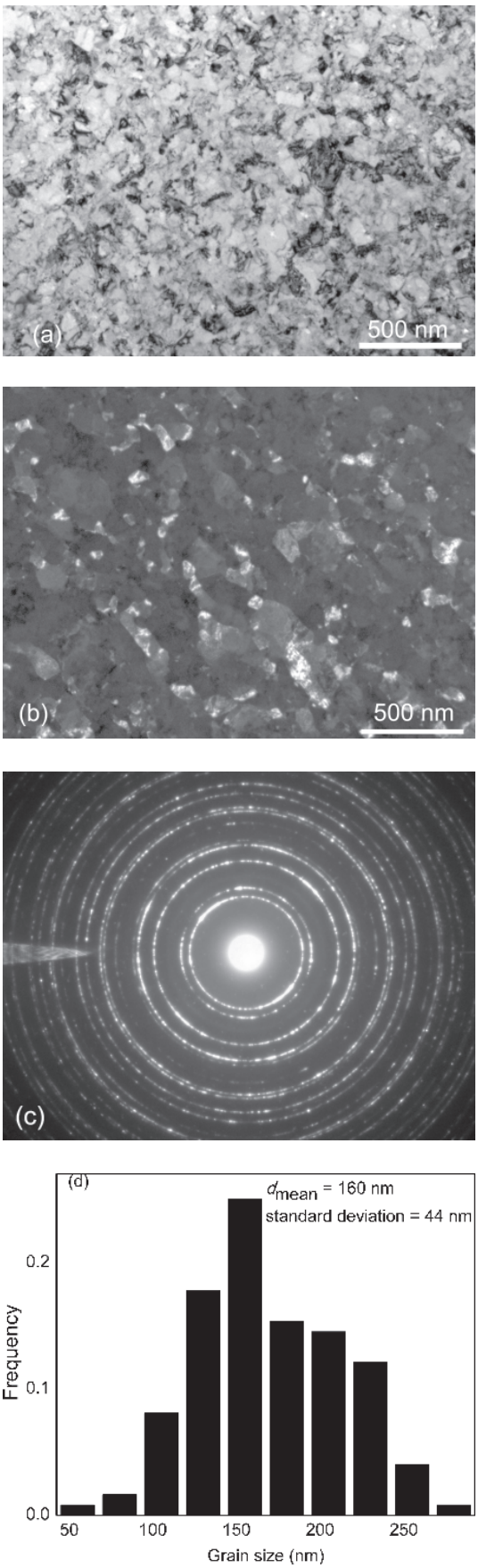

Fig. 3. TEM micrographs of Cu-77 wt.% Ni alloy homogenized at 850 °C for 500 h after HPT (8 GPa, 5 rot, 1 rpm): (a) Bright field; (b) Dark field; (c) Diffraction pattern. (d) Histogram for the distribution of grain size *d*.

transforms into another) [76]. Such grain boundaries are frequently called non-equilibrium [78].

The commercial Nd–Fe–B-based alloy behaves differently, and not only from the mechanical point of view (Fig. 1). The starting mixture of major $Nd_2Fe_{14}B$ phase and some minor crystalline phases amorphyses during HPT (Fig. 4). The amorphous matrix contains very fine $Nd_2Fe_{14}B$ grains with a size of 5–10 nm (Fig. 4a). The radial intensity distribution corresponding to the selected area electron diffraction pattern is shown in Fig. 4c. The positions of the peaks in the plot correspond to the tetragonal $Nd_2Fe_{14}B$ phase. The profile also contains a wide amorphous halo. Using the fast Fourier transform (FFT) of the HRTEM images from Nd-rich and Fe-rich areas we can estimate the *d*-values corresponding to the halo position for two amorphous phases with different compositions, which are 0.197 nm and 0.204 nm for Fe-rich and Nd-rich areas accordingly. The careful concentration measurements also show that the samples after HPT contain two different amorphous phases, Fe-rich and Nd-rich ones (Fig. 5). The sharp interface can be seen in the concentration profile between Fe-rich and Nd-rich amorphous phases (Fig. 5).

Figure 6a shows the dependence of the lattice parameter (measured by XRD) in Cu-4.9 wt.% Co alloy annealed at 570 °C for 840 h (circles) and at 1 060 °C for 10 h (squares) on the rotation speed between 0.2 and 2 rpm. The lattice parameter of the alloy annealed at 570 °C before deformation is very close to that of pure copper (diamond). With an increasing number of rotations, the lattice parameter of alloy annealed at 570 °C decreased and that of alloy annealed at 1 060 °C increased. After 5 anvil rotations (1 800°) with a speed of 1 rpm the lattice parameter in both samples becomes almost indistinguishable and corresponds to the solid solution of 2.5 wt.% Co in Cu. Figure 6c shows XRD patterns of (222) peak for the Cu-4.9 wt.% Co alloy before HPT and after HPT with 1 rpm, 5 rotations. The dotted line allows one to compare the position of the (222) peak before and after HPT. It visualizes how the (222) peaks "come together" during HPT. In other words, the composition of the solid solution in the Cu-4.9 wt.% Co alloy after the given HPT processing does not depend on the initial state prior to HPT. Thus, the steady-state with respect to the grain size, size of Co precipitates and concentration of Co in a solid solution during HPT is indeed *equifinal*. It can be seen from Fig. 6a that the lattice parameter after 5 anvil rotations is almost constant between 0.2 and 2 rpm. This means that the equifinal state in Cu–Co alloys is rather insensitive not only to the starting state but also to the strain rate.

Figure 6b shows the dependence of the lattice parameter (measured by XRD) in Cu-77 wt.% Ni alloy on the HPT pressure between 3 and 8 GPa (5 rotations, 1 rpm). Open circles show the lattice spacing in the solid solution after homogenization at 850 °C for 500 h. HPT leads to the dissolution of the homogeneous solid solution into two fcc-phases, Cu-rich (filled diamonds) and Ni-rich (filled circles) ones. It can be seen from Fig. 6b that the lattice parameter in Cu-rich and Ni-rich phases after 5 anvil rotations with a speed of 1 rpm is almost constant between 3 and 8 GPa. This means that the steady-state in Cu–Ni alloys is rather insensitive to the HPT pressure.

Figure 7a shows the Cu-rich part of the Cu–Co phase diagram [68]. Open circle corresponds to the composition of the Cu-4.9 wt.% Co alloy annealed at 570 °C for 840 h.

International Journal of Materials Research downloaded from www.hanser-elibrary.com by KIT - Karlsruher Institut für Technologie on July 11, 2015
For personal use only.

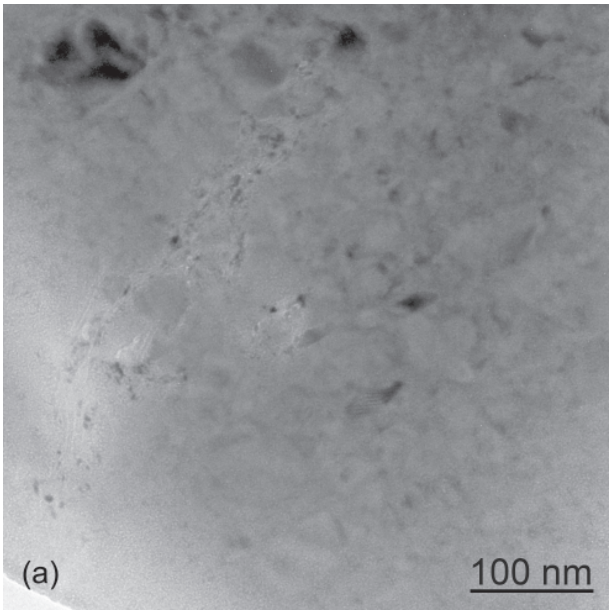

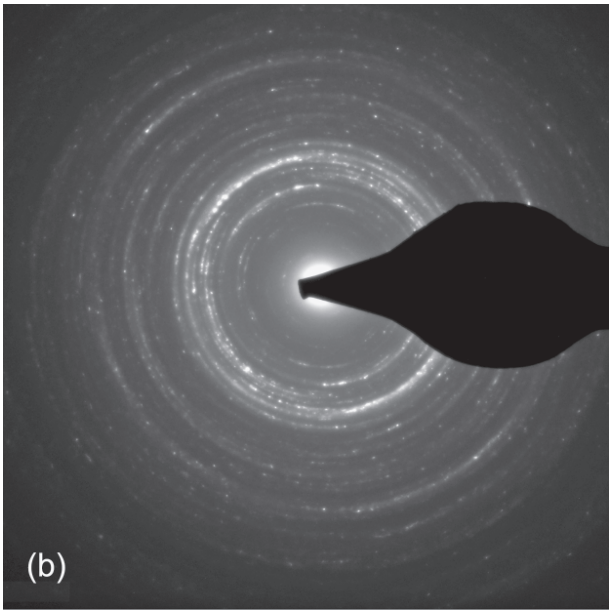

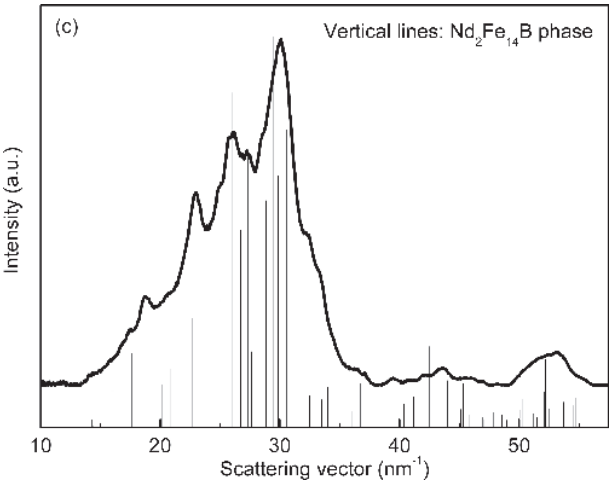

Fig. 4. (a) Bright filed TEM micrograph of HPT-deformed commercial Nd–Fe–B-based alloy. (b) Electron diffraction pattern. (c) Radial distribution of scattered electrons. The amorphous halo and lines of $Nd_2Fe_{14}B$ phase are visible.

Open square corresponds to the composition of the Cu-4.9 wt.% Co alloy annealed at 1 060 °C for 10 h. Filled circles and squares correspond to the composition of Cu-based matrix in the Cu-4.9 wt.% Co alloy after HPT (5 GPa, 5 rotations) with different rotation speed between 0.2 and 2 rpm. The filled points "sit" on the solvus line at T_{eff} = 890 ± 30 °C. This means that the composition of Cu-matrix and the amount of Co-precipitates after HPT of both Cu-4.9 wt.% Co alloys is the same as if they had been annealed at T_{eff} = 890 ± 30 °C. However, by defining of T_{eff} using the equilibrium phase diagrams one should not forget the possible influence of grain boundary segregation. The alloys after HPT have very high specific area of grain boundaries and interphase boundaries. In the case of strong GB segregation, the total solubility of a second component can strongly increase [28, 79].

Figure 7b shows the Cu–Ni phase diagram [68]. Open circle corresponds to the composition of the Cu-77 wt.% Ni alloy homogenized at 850 °C for 500 h. Filled diamonds and circles show the composition of two homogeneous fcc

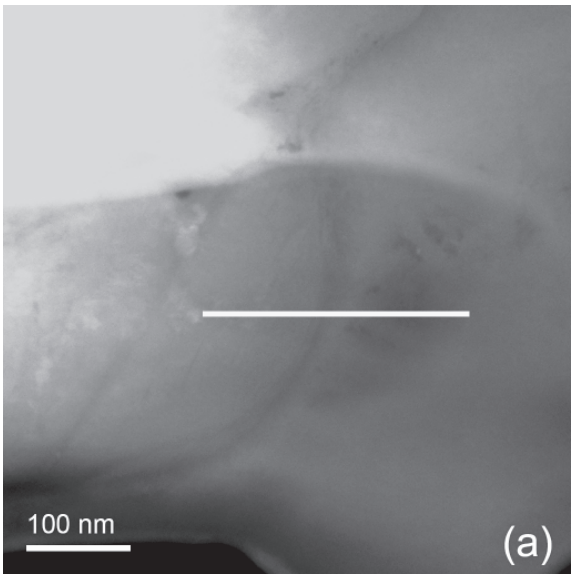

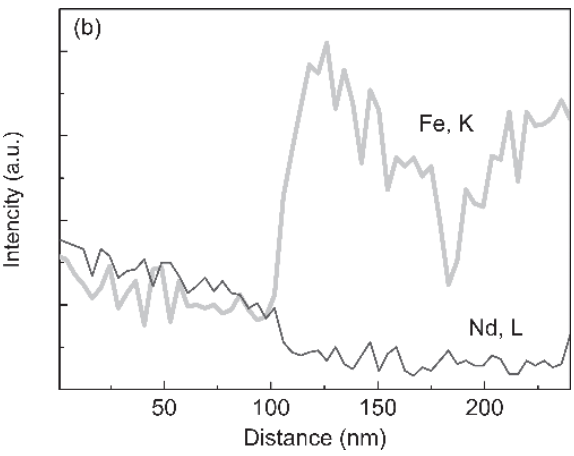

Fig. 5. (a) *Z*-contrast image obtained by HAADF STEM showing of the Nd-rich (left) and Fe-rich (right) amorphous phases in the HPT-deformed commercial Nd–Fe–B-based alloy. (b) Intensity of Fe-K (thick line) and Nd-L (thin line) EDS peaks. The position of the line profile is shown in Fig. 5a.

International Journal of Materials Research downloaded from www.hanser-elibrary.com by KIT - Karlsruher Institut für Technologie on July 11, 2015
For personal use only.

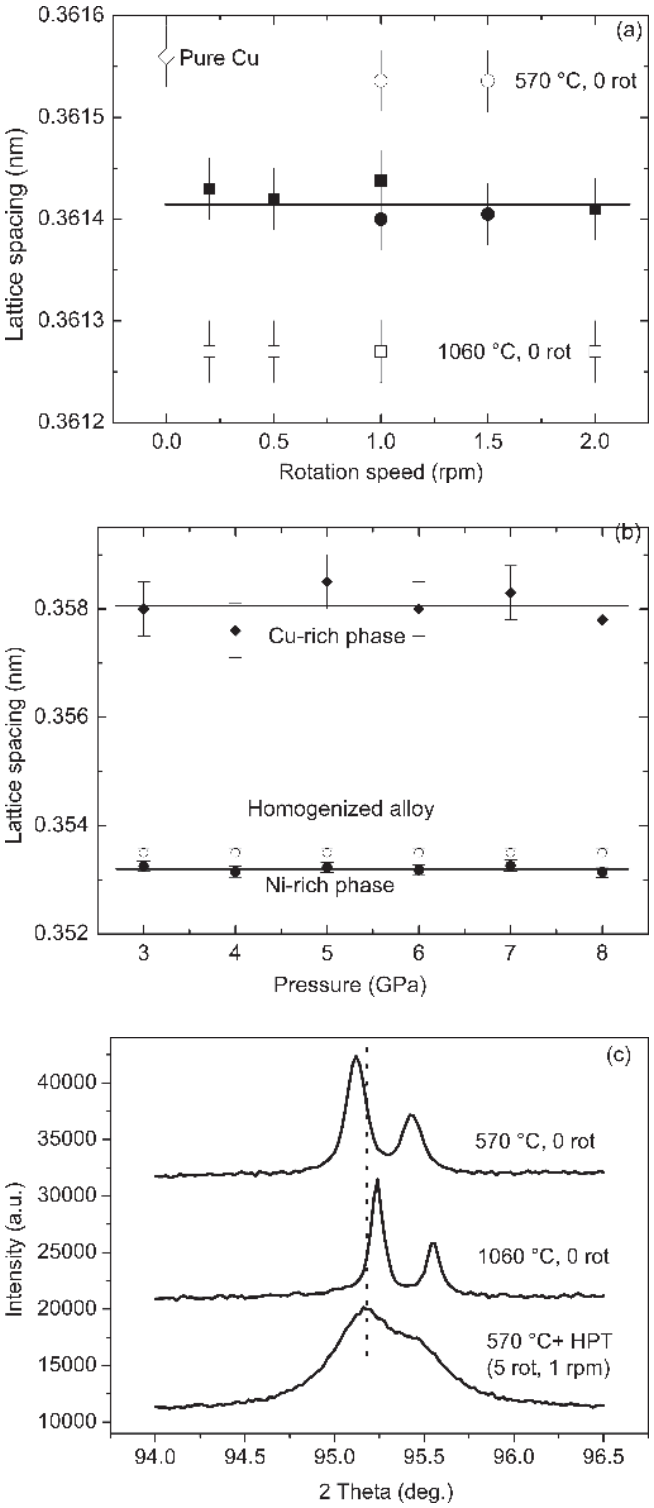

Fig. 6. (a) Dependence of the lattice parameter (measured by XRD) in Cu-4.9 wt.% Co alloy annealed at 570 °C for 840 h (circles) and at 1 060 °C for 10 h (squares) on the rotation speed between 0.2 and 2 rpm. The lattice parameter for pure Cu is given for comparison and shown by the open diamond. (b) Dependence of the lattice parameter (measured by XRD) in Cu-77 wt.% Ni alloy on the HPT pressure between 2 and 8 GPa (5 rotations, 1 rpm). Open circles show the lattice spacing in the solid solution after homogenization at 850 °C for 500 h before HPT. After HPT appear Cu-rich (filled diamonds) and Ni-rich (filled circles) phases appear. (c) XRD patterns for the Cu-4.9 wt.% Co alloy annealed at 570 °C (top) and at 1 060 °C (middle) before HPT and annealed at 570 °C after HPT with 1 rpm, 5 rot (bottom). Dotted line allows to compare the position of (222) peak after HPT with its positions before HPT.

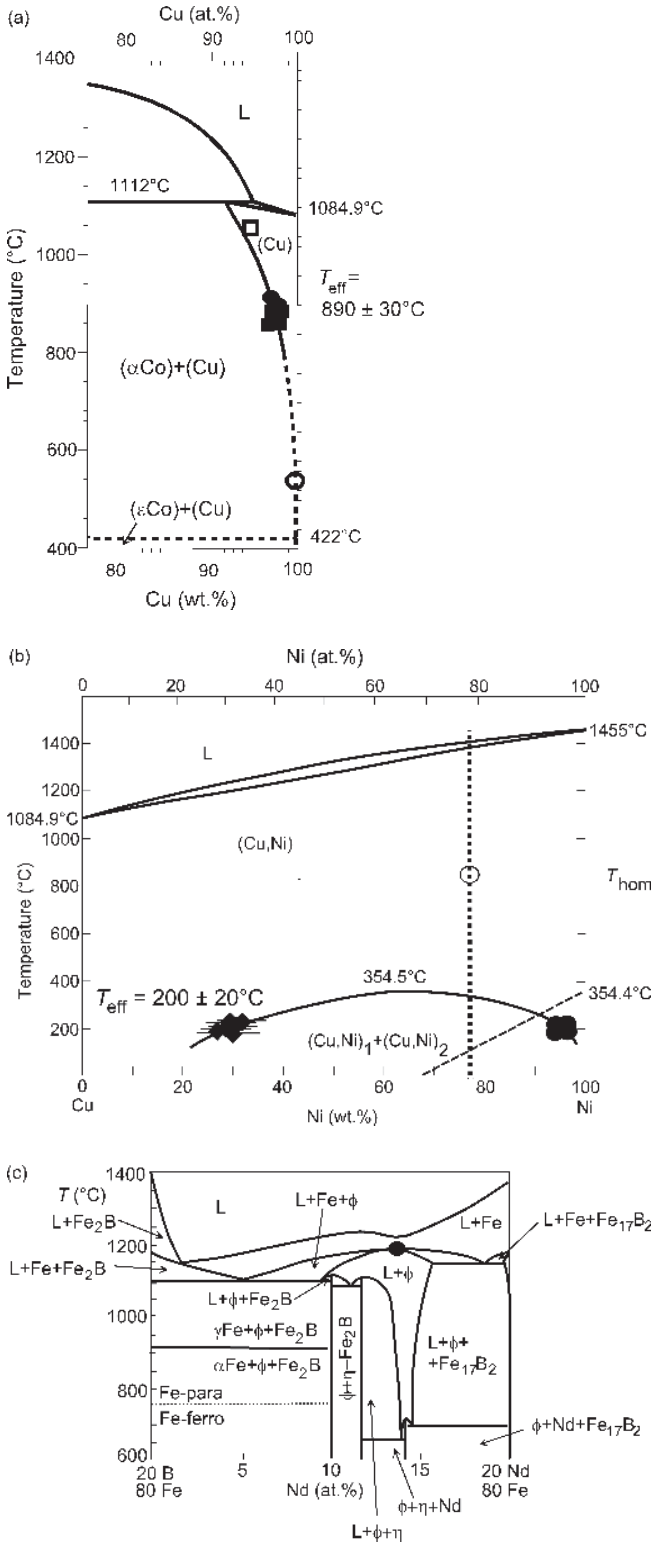

Fig. 7. (a) Cu-rich part of the Cu–Co phase diagram [68]. Open circle corresponds to the composition of the Cu-4.9 wt.% Co alloy annealed at 570 °C for 840 h. Open square corresponds to the composition of the Cu-4.9 wt.% Co alloy annealed at 1 060 °C for 10 h. Filled circles and squares at T_{eff} = 890 ± 30 °C correspond to the composition of Cu-based matrix in the Cu-4.9 wt.% Co alloy after HPT (5 GPa, 5 rotations) with different rotation speed between 0.2 and 2 rpm. (b) Cu–Ni phase diagram [68]. Open circle corresponds to the composition of the Cu-77 wt.% Ni alloy (dotted vertical line) homogenized at 850 °C for 500 h. Filled diamonds and circles show the composition of two homogeneous fcc solid solutions at T_{eff} = 200 ± 20 °C. (c) The 80 at.% Fe section of the Nd–Fe–B phase diagram [79–82]. Large filled circle shows the effective temperature T_{eff} = 1 170 ± 30 °C.

International Journal of Materials Research downloaded from www.hanser-elibrary.com by KIT - Karlsruher Institut für Technologie on July 11, 2015
For personal use only.

solid solutions, namely Cu-rich and Ni-rich ones, respectively. They appear after HPT as a result of quick decomposition of homogeneous Cu-77 wt.% Ni fcc solid solution. The filled points "sit" on the line of the (Cu, Ni) ↔ (Cu, Ni)$_1$ + (Cu, Ni)$_2$ decomposition dome at T_{eff} = 200 ± 20 °C. This means that the composition of Cu-rich and Ni-rich phases is the same as if they had been annealed at T_{eff} = 200 ± 20 °C.

The situation in Nd–Fe–B-based alloy is more complicated. The strong external forces acting during HPT also caused the phase transformation in the material, namely the formation of two different amorphous phases from crystalline ones and very strong refinement of remaining $Nd_2Fe_{14}B$ grains. Historically, such unusual behaviour was first observed in materials under severe irradiation [62]. Martin proposed for the first time a simplified mean-field description of solid solutions subjected to irradiation-induced atomic mixing [62, 63]. His main idea was that the forced mixing induced by irradiation emulates the increase of entropy and changes the thermodynamic potentials in the alloy. Martin also proposed for the first time to use the equilibrium phase diagram for the description of the system under irradiation, but at T_{eff} instead of the actual temperature T. For example, if the liquid phase is present in the phase diagram at T_{eff}, the amorphous phase would appear under irradiation [62, 63]. The composition of the phases after SPD allows localizing those phases in the respective equilibrium phase diagram (as we did above for the Cu–Co and Cu–Ni alloys) and estimation of effective temperature T_{eff}. In case of Nd–Fe–B-based alloy HPT leads to the formation of two amorphous phases. The Nd–Fe–B phase diagram contains two immiscible melts above 1 150 °C [80–83]. Therefore, the effective temperature is slightly above 1 150 °C and can be estimated as T_{eff} = 1 170 ± 30 °C (Fig. 7c, large filled circle).

4. Conclusions

Severe plastic deformation by HPT leads to phase transitions and strong grain refinement in several metallic alloys. SPD-treatment at ambient temperature T_{SPD} is frequently equivalent to heat treatment at a certain elevated (effective) temperature T_{eff}. The steady-state is reached during HPT after a certain number of anvil rotations. The structure and properties of a material in a steady state (including composition of phases) do not depend on those in the starting state before HPT, in other words they are equifinal. The composition of phases in Cu–Ni, Co–Cu and Nd–Fe–B-based alloys after HPT corresponds to the states at 200, 890 and 1 170 °C, respectively, and is rather insensitive to the HPT rate (between 0.2. and 2 rpm) and pressure (between 3 and 8 GPa).

The work was partially supported by the Russian Foundation for Basic Research (grants 14-48-03598, 14-08-00972, 15-03-01127 and 13-08-90422), Government of Moscow Region, the Russian Federal Ministry for Education and Science (grants 14.A12.31.0001 and Increase Competitiveness Program of NUST«MISiS» K2-2014-013), Programme "New materials" of RAS, Karlsruhe Nano Micro Facility operated by the Karlsruhe Institute of Technology, The Allianz Industrie Forschung (grant FVA 631 II), and Polish National Science Centre (grant DEC-2011/01/M/ST8/07822).

References

[1] X. Sauvage, A. Chbihi, X. Quelennec: J. Phys. 240 (2010) 012003. DOI:10.1088/1742-6596/240/1/012003
[2] B.B. Straumal, A.A. Mazilkin, B. Baretzky, E. Rabkin, R.Z. Valiev: Mater. Trans. 53 (2012) 63. DOI:10.2320/matertrans.MD201111
[3] C. Suryanarayana, F.H. Froes: J. Mater. Res. 5 (1990) 1880. DOI:10.1557/JMR.1990.1880
[4] E.I. Teitel', L.S. Metlov, D.V. Gunderov, A.V. Korznikov: Phys. Metall. Metallogr. 113 (2012) 1162. DOI:10.1134/S0031918X12120095
[5] W. Lojkowski, M. Djahanbakhsh, G. Burkle, S. Gierlotka, W. Zielinski, H.J. Fecht: Mater. Sci. Eng. A 303 (2001) 197. DOI:10.1016/S0921-5093(00)01947-X
[6] K. Hono, M. Ohnuma, M. Murayama, S. Nishida, A. Yoshie, T. Takahashi: Scr. Mater. 44 (2001) 977. DOI:10.1016/S1359-6462(00)00690-4
[7] A. Taniyama, T. Takayama, M. Arai, T. Hamada: Scr. Mater. 51 (2004) 53. DOI:10.1016/j.scriptamat.2004.03.018
[8] V.G. Gavriljuk: Mater. Sci. Eng. A 345 (2003) 81. DOI:10.1016/S0921-5093(02)00358-1
[9] X. Sauvage, X. Quelennec, J.J. Malandain, P. Pareige: Scr. Mater. 54 (2006) 1099. DOI:10.1016/j.scriptamat.2005.11.068
[10] V.A. Teplov, V.P. Pilugin, V.S. Gaviko, E.G. Chernyshov: Phil. Mag. B 68 (1993) 877. DOI:10.1080/13642819308217944
[11] V.V. Stolyarov, R. Lapovok, I.G. Brodova, P.F. Thomson: Mater. Sci. Eng. A 357 (2003) 159. DOI:10.1016/S0921-5093(03)00215-6
[12] X. Sauvage, F. Wetscher, P. Pareige: Acta Mater. 53 (2005) 2127. DOI:10.1016/j.actamat.2005.01.024
[13] B.B. Straumal, B. Baretzky, A.A. Mazilkin, F. Phillipp, O.A. Kogtenkova, M.N. Volkov, R.Z. Valiev: Acta Mater. 52 (2004) 4469. DOI:10.1016/j.actamat.2004.06.006
[14] A.A. Mazilkin, B.B. Straumal, E. Rabkin, B. Baretzky, S. Enders, S.G. Protasova, O.A. Kogtenkova, R.Z.Valiev: Acta Mater. 54 (2006) 3933. DOI:10.1016/j.actamat.2006.04.025
[15] B.B. Straumal, S.G. Protasova, A.A. Mazilkin, E. Rabkin, D. Goll, G. Schütz, B. Baretzky, R.Z. Valiev: J. Mater. Sci. 47 (2012) 360. DOI:10.1007/s10853-011-5805-0
[16] C.M. Cepeda-Jiménez, J.M. García-Infanta, A.P. Zhilyaev, O.A. Ruano, F. Carreño: J. Alloys Compd. 509 (2011) 636. DOI:10.1016/j.jallcom.2010.09.122
[17] Y. Ivanisenko, I. MacLaren, X. Sauvage, R.Z. Valiev, H.-J. Fecht: Acta Mater. 54 (2006) 1659. DOI:10.1016/j.actamat.2005.11.034
[18] X. Sauvage, Y. Ivanisenko: J. Mater. Sci. 42 (2007) 1615. DOI:10.1007/s10853-006-0750-z
[19] Y. Ivanisenko, W. Lojkowski, R.Z. Valiev, H.J. Fecht: Acta Mater. 51 (2003) 5555. DOI:10.1016/S1359-6454(03)00419-1
[20] V.V. Sagaradze, S.V. Morozov, V.A. Shabashov, L.N. Romashev, R.I. Kuznetsov: Phys. Met. Metall. 66 (1988) 328.
[21] B.B. Straumal, A.A. Mazilkin, S.G. Protasova, S.V. Dobatkin, A.O. Rodin, B. Baretzky, D. Goll, G. Schütz: Mater. Sci. Eng. A 503 (2009) 185. DOI:10.1016/j.msea.2008.03.052
[22] V.V. Sagaradze, V.A. Shabashov: Nanostruct. Mater. 9 (1997) 681. DOI:10.1016/S0965-9773(97)00053-6
[23] M. Murayama, K. Hono, Z. Horita: Mater. Trans. – JIM 40 (1999) 938. DOI:10.2320/matertrans1989.40.938
[24] S. Ohsaki, S. Kato, N. Tsuji, T. Ohkubo, K. Hono: Acta Mater. 55 (2007) 2885. DOI:10.1016/j.actamat.2006.12.027
[25] X. Sauvage, R. Pippan: Mater. Sci. Eng. A 410–411 (2005) 345. DOI:10.1016/j.msea.2005.08.122
[26] X. Sauvage, C. Genevois, G. Da Costa, V. Pantsyrny: Scr. Mater. 61 (2009) 660. DOI:10.1016/j.scriptamat.2009.06.007
[27] X. Sauvage, W. Lefebvre, C. Genevois, S. Ohsaki, K. Hono: Scr. Mater. 60 (2009) 1056. DOI:10.1016/j.scriptamat.2009.02.019
[28] B.B. Straumal, S.V. Dobatkin, A.O. Rodin, S.G. Protasova, A.A. Mazilkin, D. Goll, B. Baretzky: Adv. Eng. Mater. 13 (2011) 463. 201000312. DOI:10.1002/adem.201000312
[29] A.V. Korznikov, O. Dimitrov, G.F. Korznikova, J.P. Dallas, A. Quivy, R.Z. Valiev, A. Mukherjee: Nanostruct. Mater. 11 (1999) 17. DOI:10.1016/S0965-9773(98)00157-3
[30] A.V. Korznikov, G. Tram, O. Dimitrov, G.F. Korznikova, S.R. Idrisova, Z. Pakiela: Acta Mater. 49 (2001) 663. DOI:10.1016/S1359-6454(00)00345-1
[31] C. Rentenberger, H.P. Karnthaler: Acta Mater. 56 (2008) 2526. DOI:10.1016/j.actamat.2008.01.035

International Journal of Materials Research downloaded from www.hanser-elibrary.com by KIT - Karlsruher Institut für Technologie on July 11, 2015
For personal use only.

[32] A.V. Sergueeva, C. Song, R.Z. Valiev, A.K. Mukherjee: Mater. Sci. Eng. A 339 (2003) 159. DOI:10.1016/S0921-5093(02)00122-3
[33] S.D. Prokoshkin, I.Yu. Khmelevskaya, S.V. Dobatkin, I.B. Trubitsyna, E.V. Tatyanin, V.V. Stolyarov, E.A. Prokofiev: Acta Mater. 53 (2005) 2703. DOI:10.1016/j.actamat.2005.02.032
[34] X. Sauvage, L. Renaud, B. Deconihout, D. Blavette, D.H. Ping, K. Hono: Acta Mater. 49 (2001) 389. DOI:10.1016/S1359-6454(00)00338-4
[35] T. Miyazaki, D. Terada, Y. Miyajima, C. Suryanarayana, R. Murao, Y. Yokoyama, K. Sugiyama, M. Umemoto, T. Todaka, N. Tsuji: J. Mater. Sci. 46 (2011) 4296. DOI:10.1007/s10853-010-5240-7
[36] A.A. Mazilkin, G.E. Abrosimova, S.G. Protasova, B.B. Straumal, G. Schütz, S.V. Dobatkin, A.S. Bakai: J. Mater. Sci. 46 (2011) 4336. . DOI:10.1007/s10853-011-5304-3
[37] V.V. Stolyarov, D.V. Gunderov, A.G. Popov, V.S. Gaviko, A.S. Ermolenko: J. Alloys Compd. 281 (1998) 69. DOI:10.1016/S0925-8388(98)00774-9
[38] Y. Matsuura, S. Hirosawa, H. Yamamoto, S. Fujimira, M. Sagawa, K. Osamura: Jap. J. Appl. Phys. Part 2 – Lett. 24 (1985) L635. DOI:10.1143/JJAP.24.L635
[39] B.B. Straumal, A.A. Mazilkin, S.G. Protasova, D. Goll, B. Baretzky, A.S. Bakai, S.V. Dobatkin: Kovove Mater. – Metall. Mater. 49 (2011) 17.
[40] Á. Révész, S. Hóbor, J.L. Lábár, A.P. Zhilyaev, Zs. Kovácz: J. Appl. Phys. 100 (2006) 103522. DOI:10.1063/1.2388868
[41] I. MacLaren, Y. Ivanisenko, R.Z. Valiev, H.J. Fecht: J. Phys. 26 (2006) 335. DOI:10.1088/1742-6596/26/1/058
[42] Y. Ivanisenko, I. MacLaren, X. Sauvage, R.Z. Valiev, H.J. Fecht: Sol. State Phenom. 114 (2006) 133. DOI:10.4028/www.scientific.net/SSP.114.133
[43] Y. Ivanisenko, I. MacLaren, X. Sauvage, R.Z. Valiev, H.J. Fecht: Acta Mater. 54 (2006) 1659. DOI:10.1016/j.actamat.2005.11.034
[44] A.P. Zhilyaev, I. Sabirov, G. González-Doncel, J. Molina-Aldareguía, B. Srinivasarao, M.T. Pérez-Prado: Mater. Sci. Eng. A 528 (2011) 3496. DOI:10.1016/j.msea.2011.01.062
[45] A.P. Zhilyaev, A.V. Sharafutdinov, M.T. Pérez-Prado: Adv. Eng. Mater. 12 (2010) 754. DOI:10.1002/adem.200900348
[46] A.P. Zhilyaev, F. Gálvezc, A.V. Sharafutdinov, M.T. Pérez-Prado: Mater. Sci. Eng. A 527 (2010) 3918. DOI:10.1016/j.msea.2010.02.066
[47] M.T. Pérez-Prado, A.V. Sharafutdinov, A.P. Zhilyaev: Mater. Lett. 64 (2010) 211. DOI:10.1016/j.matlet.2009.10.049
[48] M.T. Pérez-Prado, A.P. Zhilyaev: Phys. Rev. Lett. 102 (2009) 175504. DOI:10.1103/PhysRevLett.102.175504
[49] K. Edalati, Z. Horita, Y. Mine: Mater. Sci. Eng. A 527 (2010) 2136. DOI:10.1016/j.msea.2009.11.060
[50] K. Edalati, Z. Horita, S. Yagi, E. Matsubara: Mater. Sci. Eng. A 523 (2009) 277. DOI:10.1016/j.msea.2009.07.029
[51] K. Edalati, E. Matsubara, Z. Horita: Metal. Mater. Trans. A 40 (2009) 2079. DOI:10.1007/s11661-009-9890-5
[52] Y. Ivanisenko, A. Kilmametov, H. Roesner, R.Z. Valiev: Int. J. Mater. Res. 99 (2008) 36. DOI:10.3139/146.101606
[53] A.M. Glezer, M.R. Plotnikova, A.V. Shalimova, S.V. Dobatkin: Bull. Russ. Acad. Sci. Phys. 73 (2009) 1233. DOI:10.3103/S1062873809090123
[54] S. Hóbor, Á. Révész, A.P. Zhilyaev, Zs. Kovácz: Rev. Adv. Mater. Sci. 18 (2008) 590.
[55] Zs. Kovács, P. Henits, A.P. Zhilyaev, Á.Révész: Scr. Mater. 54 (2006) 1733. DOI:10.1016/j.scriptamat.2006.02.004
[56] G.E. Abrosimova, A.S. Aronin, S.V. Dobatkin, S.D. Kaloshkin, D.V. Matveev, O.G. Rybchenko, E.V. Tatyanin, I.I. Zverkova: J. Metastab. Nanocryst. Mater. 24 (2005) 69. DOI:10.4028/www.scientific.net/JMNM.24-25.69
[57] Á. Révész, E. Schafler, Zs. Kovács: Appl. Phys. Lett. 92 (2008) 011910. DOI:10.1063/1.2830992
[58] S. Hóbor, Zs. Kovács, A.P. Zhilyaev, L.K. Varga, P.J. Szabó, Á. Révész: J. Phys. 240, (2010) 012153. DOI:10.1088/1742-6596/240/1/012153
[59] S. Hóbor, Á. Révész, P.J. Szabó, A.P. Zhilyaev, V. Kovács Kis, J.L. Lábár, Zs. Kovács: J. Appl. Phys. 104 (2008) 033525. DOI:10.1063/1.2964115
[60] P. Henits, Á. Révész, A.P. Zhilyaev, Zs. Kovács: J. Alloys Compd. 461 (2008) 195. DOI:10.1016/j.jallcom.2007.07.049
[61] Zs. Kovács, P. Henits, A.P. Zhilyaev, N.Q. Chinh, Á. Révész: Mater. Sci. Forum 519–521 (2006) 1329. DOI:10.4028/www.scientific.net/MSF.519-521.1329
[62] G. Martin: Phys. Rev. B 30 (1984) 1424. DOI:10.1103/PhysRevB.30.1424
[63] P. Bellon, G. Martin: Nucl. Instr. Meth. Phys. Res. B 19 (1987) 619. DOI:10.1016/S0168-583X(87)80124-6
[64] B.B. Straumal, L.M. Klinger, L.S. Shvindlerman: Scr. Metal. 17 (1983) 275. DOI:10.1016/0036-9748(83)90156-4
[65] D.A. Molodov, B.B. Straumal, L.S. Shvindlerman: Scr. Metal. 18 (1984) 207. DOI:10.1016/0036-9748(84)90509-X
[66] B.B. Straumal, A.R. Kilmametov, Yu.O. Kucheev, L. Kurmanaeva, Yu. Ivanisenko, B. Baretzky, A. Korneva, P. Zięba, D.A. Molodov: Mater. Lett. 118 (2014) 111. DOI:10.1016/j.matlet.2013.12.042
[67] L. von Bertalanffy: Human Biology 23 (1951) 302.
[68] T.B. Massalski et al. (Eds): Binary Alloy Phase Diagrams, ASM International, Materials Park, OH (1993).
[69] A.A. Mazilkin, B.B. Straumal, M.V. Borodachenkova, R.Z. Valiev, O.A. Kogtenkova, B. Baretzky: Mater. Lett. 84 (2012) 63. DOI:10.1016/j.matlet.2012.06.026
[70] R.Z. Valiev, T.G. Langdon: Prog. Mater. Sci. 51 (2006) 881. DOI:10.1016/j.pmatsci.2006.02.003
[71] R. Valiev, R. Islamgaliev, I. Alexandrov: Prog. Mater. Sci. 45 (2000) 103. DOI:10.1016/S0079-6425(99)00007-9
[72] B.B. Straumal, S.G. Protasova, A.A. Mazilkin, E. Rabkin, D. Goll, G. Schütz, B. Baretzky, R. Valiev: J. Mater. Sci. 47 (2012) 360. DOI:10.1007/s10853-011-5805-0
[73] N. Lugo, N. Llorca, J.M. Cabrera, Z. Horita: Mater. Sci. Eng. A 477 (2008) 366. DOI:10.1016/j.msea.2007.05.083
[74] J. Čížek, M. Janeček, O. Srba, R. Kužel, Z. Barnovská, I. Procházka, S. Dobatkin: Acta Mater. 59 (2011) 2322. DOI:10.1016/j.actamat.2010.12.028
[75] X.Z. Liao, Y.H. Zhao, Y.T. Zhu, R.Z. Valiev, D.V. Gunderov: J. Appl. Phys. 96 (2004) 636. DOI:10.1063/1.1757035
[76] B.B. Straumal, A.R. Kilmametov, A.A. Mazilkin, L. Kurmanaeva, Y. Ivanisenko, A. Korneva, P. Zięba, B. Baretzky: Mater. Lett. 138 (2014) 255. DOI:10.1016/j.matlet.2014.10.009
[77] B. Straumal, R. Valiev, O. Kogtenkova, P. Zieba, T. Czeppe, E. Bielanska, M. Faryna: Acta Mater. 55 (2008) 6123. DOI:10.1016/j.actamat.2008.08.021
[78] X. Sauvage, G. Wilde, S.V. Divinski, Z. Horita, R.Z. Valiev: Mater. Sci. Eng. A 540 (2012) 1. DOI:10.1016/j.msea.2012.01.080
[79] B.B. Straumal, S.A. Polyakov, L.-S. Chang, E.J. Mittemeijer: Int. J. Mater. Res. 98 (2007) 451. DOI :. DOI:10.3139/146.101502
[80] G. Thomas, H. Mori, H. Fujita: Scr. Metal. 16 (1982) 589. DOI:10.1016/0036-9748(82)90276-9
[81] Z.S. Ji, M.L. Hu, X.P. Zheng: J. Mater. Sci. Technol. 23 (2007) 247. DOI:10.1179/174328407X154356
[82] Y.A. Shatilla, E.P. Loewen: Nucl. Technol. 151 (2005) 239.
[83] M. Sagawa, S. Fujimura, N. Togawa, H. Yamamoto, Y. Matsuura: J. Appl. Phys. 55 (1984) 2083. DOI:10.1063/1.333572

(Received November 3, 2014; accepted January 12, 2015; online since April 2, 2015)

Correspondence address

Prof. Dr. Boris Straumal
Institute of Solid State Physics
Russian Academy of Sciences
Ac. Ossipyan str. 2
142432 Chernogolovka
Russia
Tel.: +7 49652 28300
Fax: +7 49652 28160
E-mail: straumal@issp.ac.ru

Bibliography
DOI 10.3139/146.111215
Int. J. Mater. Res. (formerly Z. Metallkd.)
106 (2015) 7; page 657–664
© Carl Hanser Verlag GmbH & Co. KG
ISSN 1862-5282